Green Chemistry

PAPER

View Article Online
View Journal | View Issue

Cite this: *Green Chem.*, 2021, **23**, 856

Liquid nanostructure of choline lysinate with water and a model lignin residue†

Haihui Joy Jiang, [a] Shurui Miao, [a] Silvia Imberti, ‡[b] Blake A. Simmons, [c] Rob Atkin [d] and Gregory G. Warr *[a]

Received 28th October 2020,
Accepted 22nd December 2020

DOI: 10.1039/d0gc03664a

rsc.li/greenchem

The structure of the ionic liquid choline lysinate ([Ch][Lys]) and its water mixtures, including a dissolved model lignin residue, guaiacol, is revealed at atomic and nanoscale resolution using neutron diffraction. The performance of [Ch][Lys] for biomass pretreatment depends on both its detailed H-bonding capacity and bicontinuous polar/apolar nanostructure, which is stabilised by lysinate adopting an H-bonded cyclic conformer that enhances its amphiphilicity. These features are heightened by the addition of water, which forms nanoscale pockets but also extends the H-bonding network within the IL polar domains while largely preserving its bicontinuous nanostructure, rendering the ionic liquid–water mixture an effective solvent for organic molecules bearing various functional groups. A model representative lignin compound, guaiacol, is found to H-bond through its phenol group to both the anion and water, destabilising the lysinate cyclic conformer and altering the liquid nanostructure.

Introduction

Ionic liquids (ILs) possess many remarkable physiochemical properties including high solubilities for many compounds that are insoluble in molecular solvents. This makes certain ILs attractive candidates for effecting dissolution and fractionation of lignin during the pretreatment of biomass, which is a key step towards a commercially viable and sustainable biorefinery process.[1] Although a range of ILs are effective for lignin extraction, many suffer from disadvantages like high toxicity and high cost, which make them less desirable for industrial uses.[2] Bio-based solvents, such as choline amino acid ionic liquids, are non-toxic, renewable and inexpensive. They are the next generation of sustainable solvents for biomass processing and lignin dissolution.

Liu *et al.* have reported non-toxic and biodegradable ILs containing cholinium as the cation and amino acids as anions.[3] With up to 20% w/w water, the delignification yield from these amino acid-based ILs is maintained.[4] Moisture tolerance is also critical for cost-effective IL applications, as the complete removal of water from ILs and biomass requires energy, and because water–IL mixtures are less expensive than pure ILs. Among the eight bio-based ILs that have low viscosity and high lignin selectivity at ambient temperature, cholinium lysinate ([Ch][Lys]) demonstrates the highest potential as a pretreatment solvent.[5] Lignin accumulates in [Ch][Lys] at a constant rate over five extraction cycles without purification. Sun *et al.* used quantum calculations to show the high solvation capacity of [Ch][Lys] was a consequence of the higher hydrogen bonding basicity of lysinate compared to simpler anions like acetate.[6] However, how these bio-based ILs solubilise the complex structures within lignin, including polar, aromatic, and non-polar moieties, and how water influences the lignin extraction process are not understood at the nanoscale. A molecular understanding of the effect of solvent structure, solvent–solute interactions and how additional water molecules affect solvent–solute interactions is necessary for designing and developing subsequent novel ILs for biomass pretreatment.

Here we investigate the structure of liquid [Ch][Lys], the effect of added water, and the relationship between ion structure and the solubility of a model lignin residue to identify key intermolecular interactions and thus develop a design framework to optimise extraction efficiency. We first investigate the bulk structure of pure [Ch][Lys] and identify the key intermolecular interactions that determine its nanostructure. As [Ch][Lys], and other ILs used for biomass processing, are typically not dry, we then show how added water affects the liquid

[a]*School of Chemistry and Sydney Nano Institute, The University of Sydney, NSW 2006, Australia. E-mail: gregory.warr@sydney.edu.au*
[b]*STFC, ISIS Neutron and Muon Source, Rutherford Appleton Laboratory, Didcot OX11 0QX, UK*
[c]*Joint BioEnergy Institute, Lawrence Berkeley National Laboratory, Berkeley, CA 94720, USA*
[d]*School of Molecular Sciences, The University of Western Australia, WA 6009, Australia*

†Electronic supplementary information (ESI) available. See DOI: 10.1039/d0gc03664a

‡Current address: Global Journals Development, ACS International Ltd., Oxford OX2 0QS, United Kingdom.

structure using a 1 : 5 mol : mol [Ch][Lys] : H_2O mixture (*i.e.* 26.5% w/w water), chosen based on effective formulations for biomass processing.[4,7,8] The role of IL nanostructure and interactions as a biomass processing solvent is then explored by adding the representative small molecule lignin fragment, guaiacol, to the system, following our previous approach using protic ionic liquids.[9,10] We compare the nanostructure of [Ch][Lys] to previously studied primary and secondary ammonium protic ILs, to identify the unique characteristics key for biomass processing.

Experimental methods

The synthesis of cholinium lysinate ([Ch][Lys]) was modified from published literature.[4] A choline hydroxide solution (Sigma, 46 wt% in water) was diluted to 10 wt%, and added dropwise to L-lysine monohydrate powder (>97%, Sigma) with stirring, at 1 : 1 molar ratio at room temperature overnight. Water was removed under reduced pressure at 40 °C. The acid–base ratio was checked by ^{1}H-NMR and ^{13}C-NMR, and a small amount of the base or the acid was added and stirred to neutrality. The IL was stirred and dried under high vacuum (0.05 mbar, 5 days) to further reduce the water content to <0.5 wt%. [Ch][Lys] was mixed with water (at 1 : 5 molar ratio, with various deuterations) for neutron experiments. The water content of IL–water samples was confirmed by Karl-Fischer (±0.1 wt%).

To prepare deuterated choline amino-acid based ILs and their mixtures for neutron experiments, d_9-choline chloride (d_9-ChCl) was exchanged into d_9-choline hydroxide (d_9-ChOH). Before use, ion exchange resins (Amberlite IRA-400 for hydroxide, 25 mL) were washed with concentrated NaOH aqueous solutions five times. A silver test (0.2 M $AgNO_3$ and 0.25 M HNO_3 in water) was carried out to ensure that a negligible amount of chloride residue remained on the resin. Flame photometry showed that the concentration of sodium was below 12 ppm. Resins were rinsed with deionised water until its pH reached neutral, then loaded onto a small column (1 cm radius) with deionised water as the eluent. An aqueous solution of d_9-ChCl (0.5 g solid in 10 mL of solvent) was loaded as the sample. All basic eluents with ChOH (pH > 7.5) were collected and combined. Water was partially removed on a rotary evaporator (30 mbar, 40 °C) and the volume was reduced to 30 mL. A known volume fraction of the obtained ChOH solution (*e.g.,* 1.00 mL out of 30.0 mL) was titrated with a standard acid solution (*e.g.,* 0.01 M HNO_3), showing a yield of 95%. The concentration of the ChOH solution was calculated based on the titrated yield and used for the synthesis of d_9-choline amino-acid ILs.

Fully hydrogenous ILs were prepared using hydrogenous reagents following procedures described above. Fresh deuterium oxide D_2O (Sigma, 99%) was added to a hydrogenous IL in a 10 : 1 molar ratio. For example, 1 mole of [Ch][Lys] has 5 moles of exchangeable hydrogens, requiring 50 moles of D_2O for each exchange. A D_2O–IL mixture was dried on a rotary evaporator, followed by high-vac. The exchange was performed four times for each IL. ^{1}H-NMR experiments reveal that, on average, 90% exchangeable hydrogens were replaced with deuterium.

Neutron diffraction was collected on SANDALS beamline at ISIS Neutron and Muon Source (Rutherford Appleton Laboratories, UK) employing neutron wavelengths between 0.05 and 4.95 Å, accessing a q-range from 0.05 to 50 Å^{-1}.[11] Samples were contained in null scattering $Ti_{0.68}Zr_{0.32}$ flat plate cells with total capacity of 1 mL. All samples were measured under vacuum at 296 K for 6 hours each. Mass were monitored to ensure no loss of sample under vacuum. Data reduction was performed using GUDRUN according to facility protocols.[12] The empirical potential structure refinement (EPSR) package was used to fit the normalized data.[13] The [Ch][Lys] simulation box contains 600 ion pairs and has a volume of 63 × 63 × 63 Å^3. The [Ch][Lys]–water box contains 560 ion pairs and 2800 water molecules, with a total volume of 68 × 68 × 68 Å^3. The [Ch][Lys]–water–guaiacol box contains 200 ion pairs, 1000 water molecules, and 100 guaiacol molecules, with a total volume of 50 × 50 × 50 Å^3. Atom labelling and initial Lennard-Jones parameters are provided in ESI (Table S1†). After standalone equilibration, the simulation box was simultaneously converged towards the experimental diffraction patterns with four distinct isotopic substitutions as shown in Fig. 1, and analyzed using DLPUTILS.[14]

Results and discussion

Neutron diffraction with selective hydrogen/deuterium isotopic substitutions yields multiple contrasts for otherwise identical chemical systems. Fig. 1 shows the resulting neutron diffraction patterns of neat [Ch][Lys], and of [Ch][Lys] : H_2O (1 : 5 mol : mol; 73.5% : 26.5% w/w) and [Ch][Lys] : H_2O : guaiacol (1 : 5 : 0.5 mol : mol; 62.1% : 22.4% : 15.5% w/w) mixtures, together with the atomic labelling scheme used for simulation and data analysis. These formulations were selected based on application-focused studies on using renewable IL–water mixtures for biomass processing, such as the pre-treatment of wheat straw,[4] sugar cane,[7] switchgrass and poplar.[8] Data are presented for the following contrasts: fully hydrogenous (red); deuterated exchangeable protons (green); deuterated cholinium charged centre methyl groups (blue); all deuterium except cation alkyl chain carbons (purple). After simultaneously fitting all four isotopic substitutions, good agreement is achieved between experimental data (dots) and EPSR calculation (solid lines). We first consider the structure of pure choline lysinate, then the subsequent effects of water dilution and addition of guaiacol.

Liquid structure in pure choline lysinate

Fig. 1 shows that neat [Ch][Lys] has an intense low-angle diffraction peak ('pre-peak') at 0.45 Å^{-1} (blue; repeat spacing, d = 14.0 Å) or 0.50 Å^{-1} (purple; d = 12.6 Å), which correspond to isotopic substitutions with the strongest neutron contrast between polar and non-polar groups. These repeat spacings

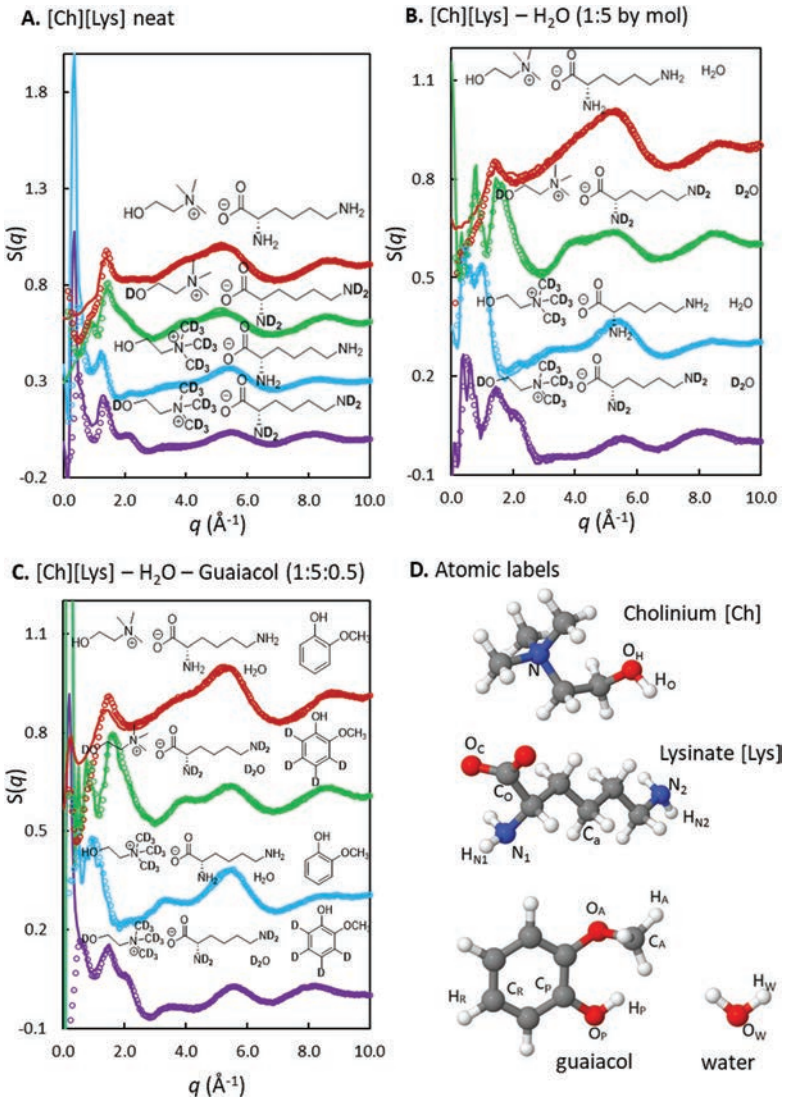

Fig. 1 Experimental neutron diffraction structure factors, $S(q)$, (points) and EPSR fitted (lines) for four different isotopic substitutions as shown for (A) choline lysinate and (B) 1 : 5 choline lysinate : water, (C) 1 : 5 : 0.5 choline lysinate : water : guaiacol at 298 K. Data are offset for clarity. (D) Atomic labelling used for EPSR modelling and subsequent analysis.

are much larger than nearest neighbour distances, which give rise to, for example, the second peak in the blue contrast at q = 1.0 Å^{-1} (d = 6.3 Å). The occurrence of such a pre-peak is a common signature of amphiphilic nanoscale structure that has been observed in a wide range of ionic liquids and their solutions,[15–19] including some choline bio-ionic liquids.[17,20–22]

In pure [Ch][Lys], EPSR fits yield low-angle peaks somewhat more intense than the experimental data, although the peak positions are consistent. This is because experimental samples contain a small amount of water due to the hygroscopicity of [Ch][Lys]. The intensity of these peaks decreases significantly upon addition of water, as seen in the [Ch][Lys]–water 1 : 5 system (Fig. 1B). This indicates that the structure of pure [Ch][Lys] has even greater nanoscale order when dry than in the presence of a small amount of water. As EPSR refines at nearest-neighbour distances, differences in intensities at the nanoscale will not influence our following interpretations.

Fig. 2 presents atom–atom pair correlation functions, $g_{ij}(r)$, spatial distributions, co-ordination numbers, and H-bond angle distributions derived from these fits for selected atoms and functional groups. Pair correlation functions show that the choline cation hydroxyl group can H-bond to the α-amino, ε-amino, or carboxylate group of the lysinate anion. Coordination numbers around the hydroxyl hydrogen (Fig. 2B) show that the most probable interaction is overwhelmingly with the carboxylate oxygen, forming H-bonds at almost a 1 : 1 stoichiometry, consistent with other cholinium-based ILs.[23–25] H-Bonding to the ε-amine is about 20% as prevalent, while there is very little hydrogen bonding to the α-amine. Corresponding spatial distribution functions (Fig. 2C) show

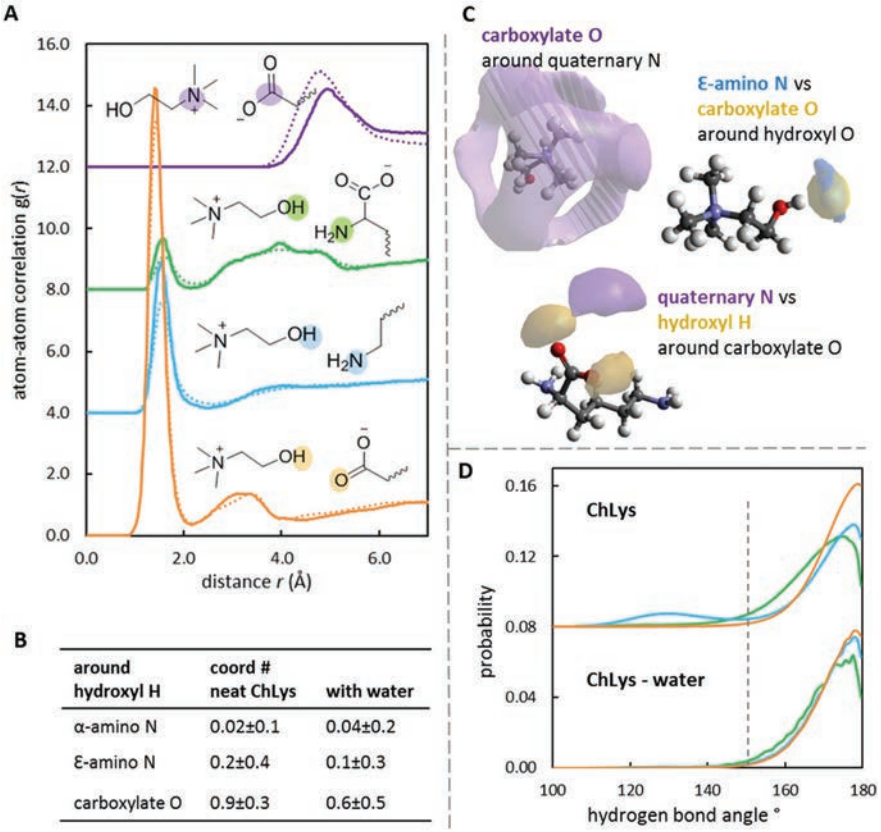

Fig. 2 A. Atom–atom pair correlation functions, $g_{ij}(r)$, in neat [Ch][Lys] (dotted lines) and 1 : 5 mol : mol [Ch][Lys]–water mixtures (solid lines). B. Coordination numbers of anion functional groups around the cation hydroxyl hydrogen in neat [Ch][Lys] and the [Ch][Lys]–water system, defined within 0–2.3 Å. C. 3D spatial distribution functions of selected [Ch][Lys] atoms, showing 20% probability surfaces. D. H-Bond angle distributions in neat [Ch][Lys] and the [Ch][Lys]–water. Structural labels and surfaces are colour coded to $g(r)$.

choline hydroxyls localised into two small, well-defined lobes (yellow) next to each carboxylate oxygen, yielding a narrow distribution of near-linear C_O–O_C···H_O–H-bond angles (Fig. 2D).

Electrostatic correlations between cation and anion charged groups (shown in purple in Fig. 2A) are less pronounced and occur at greater distance than in most primary and secondary ammonium protic ILs,[9,15,26] due to steric hindrance around the quaternary ammonium group. The carboxylate is mostly distributed homogeneously around the ammonium, but with some remnants of 3-fold symmetry from the methyl groups (Fig. 2C). The complementary spatial distribution function of the quaternary ammonium around the lysinate anion (Fig. 2C) shows that it predominantly lies between the carboxyl oxygens. Our previous study of pyrrolidinium acetate also found that its nitrogen charge centre also predominantly occurred between the two carboxylate oxygens of acetate, in that case forming an apparent bent hydrogen bond, but actually dominated by electrostatics.[9]

Lysine is not conventionally classified as having a hydrophobic sidechain, due to its polar ε-amino group. Strong electrostatic and H-bonding interactions can only generate amphiphilic nanostructure through a solvophobic effect if a non-polar group is available to create separate domains. Fig. 3 shows that lysinate adopts a wide distribution of conformers, including a significant population in which the ε-amino is closer to the carboxylate oxygen than the α-amino. The closest approach is <2 Å, suggesting an intramolecular H-bond. As shown in Fig. 3, in pure [Ch][Lys], 26% of lysinate ions are in the cyclic conformation, with at least one ε-hydrogen within 3.3 Å of the carboxylate group. Such a cyclic anion conformer exposes the non-polar tetramethylene chain, giving lysinate ions polar and non-polar ends and enabling amphiphilic nanostructure to form.

A recent study on the cryoprotective effect of lysine in aqueous solution has demonstrated lysine/lysinate mixtures can form dimers or homo-polyamide acid of lysine.[27] With the lack of a cation, a permanent charge on lysinate ions and under presence of abundant water, negligible cyclisation was reported. The existence of cyclic structures is likely due to a deficit and localisation of H-bond acceptors in [Ch][Lys], which gives rise to a highly competitive H-bond environment. Each [Ch][Lys] ion pair possesses three H-bond donors (5 hydrogen sites) and two effective H-bond acceptors (Lys-carboxylate and Ch-hydroxyl). Due to the strong association between the hydroxyl and carboxylate oxygens (Fig. 2A), all H-bond acceptors are located near the carboxylate, attracting

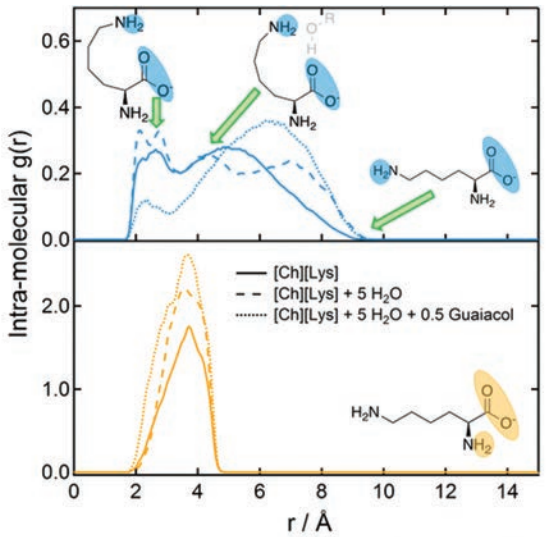

	[Ch][Lys]	[Ch][Lys]-water	[Ch][Lys]-water-guaiacol
Cyclic (< 3.3 Å)	26%	27%	9%
Water-bridged cyclic (3.3 – 5.2 Å)	----	35%	26%

Fig. 3 Intramolecular atom–atom pair correlation functions, $g_{ij}(r)$, between α- and ε-amino hydrogens and carboxyl oxygens in neat [Ch][Lys] (solid line), 1 : 5 mol : mol [Ch][Lys]–water mixtures (dashed) and 1 : 5 : 0.5 [Ch][Lys]–water–guaiacol (dotted), together with schematic representations of lysinate conformers.

H-bond donors to the same region, hence encouraging [Lys] to adopt the cyclic conformation.

The cyclic conformer population is entirely preserved upon addition of water (5 : 1 mol : mol of water : IL), a further 35% of the lysinate ions are observed to adopt a water-mediated cyclic conformation, giving rise to a second peak near 4.2 Å. After addition of guaiacol (IL : guaiacol = 1 : 0.5 mol), the fraction of both cyclic conformers decreases markedly, further validating their presence under these specific conditions. We will return to these points below.

To better visualise the nanoscale structure, in Fig. 4A we show a snapshot of a converged simulation box distinguishing charged (red) from uncharged groups (grey) of the IL. The cyclic conformation of lysinate enables pure [Ch][Lys] to form a familiar bicontinuous amphiphilic nanostructure consisting of interpenetrating domains of charged and uncharged groups whose periodicity is responsible for the scattering pre-peak.[15,18,19,28]

Fig. 4B shows the probability distributions of ions/molecules within clusters of various sizes and types present within the converged simulation box arising from different interactions between components. A cluster consists of a collection of molecules or ions whose nearest neighbour atoms all lie within a cut-off distance defined by the corresponding atom–atom pair correlation function. All clusters arising from cation and anion electrostatic interactions in pure [Ch][Lys] are near or equal to the size of the simulation box, signifying a single, continuous, polar domain. Within this domain, however, a distribution of dimers to tetramers is formed by H-bond donors and acceptors. As cluster size increases this first lies slightly above, but soon falls below the expected line for random association, or percolation threshold.[29] A single, continuous non-polar domain is similarly seen to form by the clustering of lysinate anion methylene carbons, denoted C_a (Fig. 1D; see Fig. S1† for corresponding pair correlation function).

The effect of water addition

Addition of 5 mol/mol water (26.5 wt%) has surprisingly little effect on the local structure within the IL. The average cation–anion electrostatic correlation distance increases slightly (*i.e.* the peak position is right-shifted in Fig. 2A) and decreases in intensity, but H-bonding correlations between cations and anions increase in intensity without a change in their distances. H-Bond angles between choline hydroxyl and various anion acceptor sites are all narrowly distributed around linear (Fig. 2D) in both pure IL and water solution. The sole exception is a small population of bent H-bonds to the ε-amino group (120–140°), which disappear upon water addition.

Simulation snapshots also give insights into how hydrogen/deuterium (H/D) isotopic substitution affects neutron diffraction patterns, and into the position and intensity of various peaks, including the nanostructure pre-peak. Fig. 5 qualitatively shows the different structural periodicity that arises by highlighting (*i.e.*, deuterating) three different sets of atoms within the IL–water mixture, together with their diffraction patterns. Quantitative calculations of periodicity based on the position of diffraction peaks justify simulation results. At the nanoscale, water and exchangeable protons form nano-pockets with an average size of 0.8 nm, likely enhancing the dissolution of hydrogen-bonding capable species, such as lignin residues.

If the addition of water led to a simple dilution, we would expect cation–anion correlations to change in the same direction, which is not what is observed. The intramolecular H-bond between lysinate ε-amine and carboxylate (Fig. 3) is preserved upon water addition, so that the cyclic conformer is actually slightly more prevalent. A second bent or cyclic conformer, likely due to water-bridging, also emerges as a separate peak and up to 35% of all lysinate ions can be found in this conformation. The solvophobic formation of non-polar domains thus persists upon water addition, as reflected in the persistence of the low-q pre-peak in the polar/non-polar neutron contrasts diffraction patterns (Fig. 1C), as well as in the SAXS patterns of [Ch][Lys]/water mixtures.[20] The simulation box snapshot (Fig. 4A) confirms that, upon addition of water, association of non-polar regions persists while the polar domains are swollen to accommodate water molecules (shown in blue) forming their own segregated domains.[30] The single, box-spanning domain formed by lysinate non-polar groups in pure [Ch][Lys] (Fig. 4B) is retained when water is added, although a few small clusters also occur.

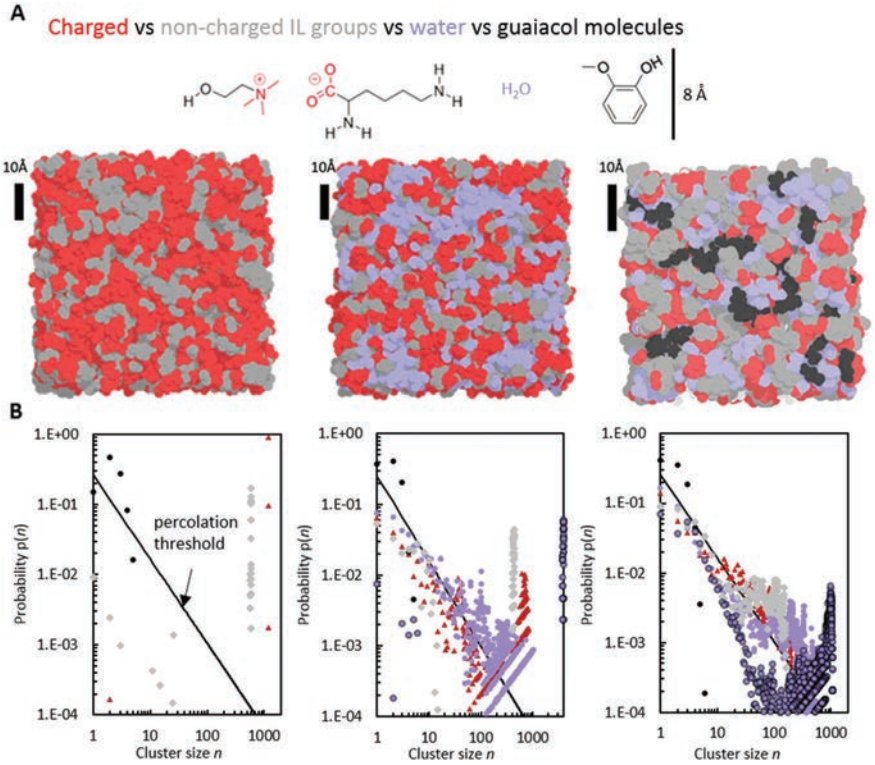

Fig. 4 A. Snapshots of converged simulation boxes of neat [Ch][Lys] (left), [Ch][Lys] : water (1 : 5 mol : mol, middle), and [Ch][Lys] : water : guaiacol (1 : 5 : 0.5, right). Colour coding distinguishes IL charged groups, uncharged groups, water, and guaiacol molecules. B. Polar clusters formed through electrostatic interactions (N–C_O, 0–6.0 Å, triangles), IL hydrogen bonding (donor–acceptor, 0–2.3 Å, circles), water clusters (H_W–O_W, 0–2.3 Å, circles), and non-polar clusters formed through lysinate methylene association (C_a–C_a, 0–5.9 Å, diamonds). Polar clusters incorporating all hydrogen bonds formed by IL and water are shown as purple circles with black borders. $p(n)$ is the fraction of ions/molecules in a cluster of size n, comprising nearest neighbours within the first coordination shell of $g(r)$. Solid line shows the theoretical percolation threshold $p(n) = n^{-1.2}$ normalised to 1.[29]

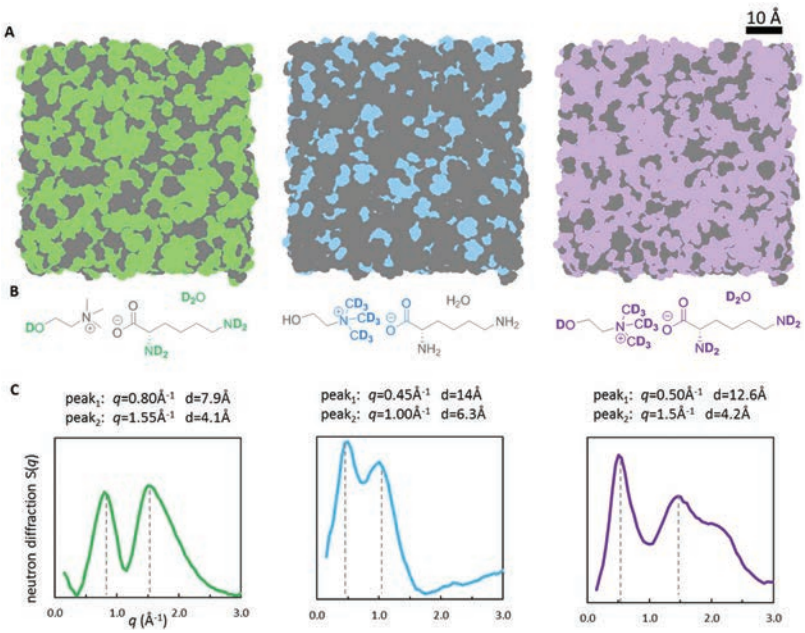

Fig. 5 Three different H/D contrasts in the [Ch][Lys]–water (1 : 5 by mole) system, showing structure at nanoscale resolution. A. Refined simulation snapshots showing contrast between deuterated and hydrogenous functional groups, according to their molecular structures B. C. Neutron diffraction patterns in the low angle range with repeating distances (Bragg spacings) calculated from peak positions.

In contrast, cluster distributions with the polar domains are strikingly different for neat [Ch][Lys] and [Ch][Lys] : H_2O 1 : 5 systems. While the continuous electrostatic network of [Ch][Lys] charged groups remains, smaller clusters ($n \approx 30$) of charged groups also appear. The small clusters formed by [Ch][Lys] H-bonding drop slightly below the percolation threshold, but the network of H-bonds including both ions and water now also forms a system-spanning, continuous domain. Water molecules form only closed clusters or 'pools' ($n < 200$), but their presence enables the ions of [Ch][Lys] to participate in a continuous, polar H-bonding network.

The hydrogen bonding of water molecules in [Ch][Lys] : H_2O 1 : 5 reveals important details about its behaviour. Atom–atom pair correlation functions around water (Fig. 6A) show that its oxygen (O_W) can H-bond with either another water molecule or a cation hydroxyl group. The water hydrogen (H_W) interacts with all three H-bond acceptors on the lysinate anion: α-amino nitrogen (N_1), ε-amino nitrogen (N_2), and carboxylate oxygen (O_C). The H-bond lengths range between 1.4–1.8 Å (Fig. 6B). The water–water correlations (Fig. 6A) exhibit peaks at 1.85 Å (hydrogen bonding) and 3.15 Å (secondary correlations), similar to those observed in pure

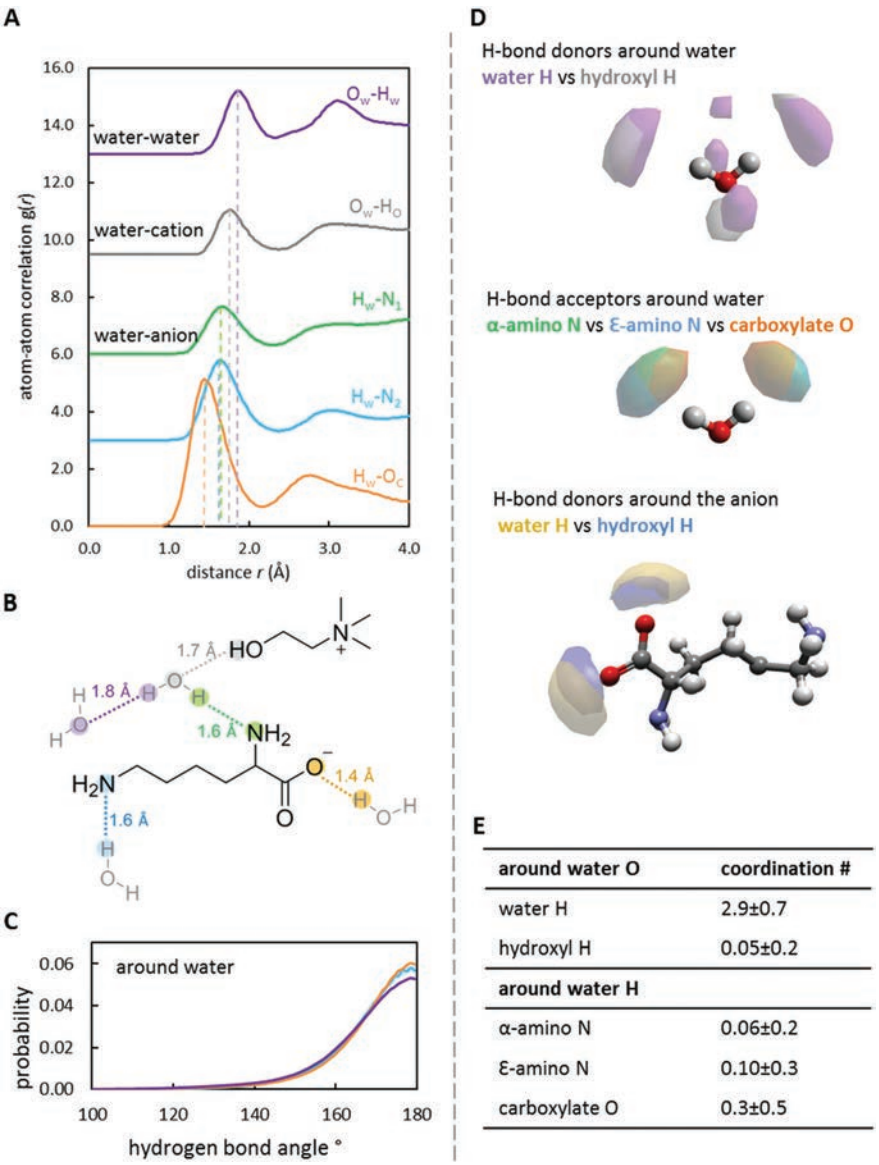

E

around water O	coordination #
water H	2.9±0.7
hydroxyl H	0.05±0.2
around water H	
α-amino N	0.06±0.2
Ɛ-amino N	0.10±0.3
carboxylate O	0.3±0.5

Fig. 6 Key H-bond characteristics in 1 : 5 mol : mol [Ch][Lys] : water. A. Atom–atom pair correlation functions, $g(r)$ between water–water (top), water-cation (second top), and several water-anion sites. B. Schematic diagram of optimal H-bonding distances derived from $g_{ij}(r)$. C. H-Bond angle distribution around water. D. 3D spatial distribution functions showing 20% probability surfaces for the competitive arrangement of H-bond donors around water; H-bond acceptors around water; H-bond donors around lysinate. E. Coordination numbers around water molecules up to 2.3 Å. Plots and structural labels are colour coded.

water (1.8 and 3.3 Å) at room temperature.[31] H-Bond angles between water molecules (shown in purple, Fig. 6C) are distributed between 160–180°, also similar to pure water.

Fig. 6D shows the geometric distribution of the various H-bond donors and acceptors around water and the anion, and competition between them. Both the water hydrogen (H_W) and the cation hydroxyl hydrogen (H_O) act as H-bond donors at multiple sites around water molecules, with geometric arrangements slightly overlapped. All three acceptor sites of the anion completely overlap and thus compete for the linear H-bonding position to water. Similarly, the distributions of water and cation hydroxyl hydrogens around the anion overlap strongly. In addition to a geometric competition between water and the cation hydroxyl group, hydrogen bond angle distributions (Fig. 6C) are similar for all donors: both species form linear hydrogen bonds.

Based on coordination numbers (Fig. 6E, Fig. S4 and Table S2†), water in this system is predominantly surrounded by other water molecules. Its dominant interaction with the IL is *via* the anion carboxylate oxygen (coordination number = 0.3 ± 0.5), with other H-bonding groups having coordination numbers <0.1. This explains the reduction in cation–anion coordination numbers upon addition of water (Fig. 2B), especially those between the carboxylate oxygen and the hydroxyl hydrogen (from 0.9 to 0.6). This is also consistent with the emergence of a second peak near 4 Å in the ε-amine/carboxylate intramolecular pair correlation function (Fig. 3). This indicates a preferred arrangement of ε-amine near the carboxylate oxygens but at a distance beyond a direct H-bond and is likely due to a water molecule bridging ε-amine hydrogen and carboxylate oxygen by acting as both a H-bond donor and acceptor. Overall, in the [Ch][Lys]–H_2O system, water molecules (up to 26.5% w/w) are accommodated into the IL H-bonding network without significantly altering its local structure, allowing the amphiphilic nanostructure to be preserved.

In terms of solvent design for the dissolution of lignin-like aromatics, the competitive hydrogen bonding between the solvent and the solute can be used to engineer amphiphilic nanostructures and strongly influence solvation.[10,25] The nanostructure of bio-ILs transitions from being "IL-like" (with 0–40 wt% water) to "water-like" (with >80 wt% water).[20] This work further highlights that the effective formulation used for biomass processing is in the "IL-like" region. The added water reduces the viscosity, reduces the cost, simplifies the process, efficiently extracts lignin residues by maintaining solvent structure at the atomic level and at the nanoscale.

Guaiacol dissolution and solvation as a model for lignin

Guaiacol is one of the canonical depolymerization products of lignin,[32,33] which is a major component of lignocellulosic biomass, that we have used to investigate ILs as potential biomass solvents in earlier work.[3,10,34] A snapshot of the refined simulation box, shown in Fig. 4A (right), helps to visualise the distribution of guaiacol molecules (15.5 wt%, shown in black) and how they influence the solvent structure. Guaiacol does not aggregate in solution at this concentration. Fig. 4B shows that guaiacol is readily accommodated within the solvent: both the electrostatic and H-bonding interactions between IL ions form a continuous polar network that is virtually the same as that in [Ch][Lys]–water (73.5% : 26.5% by wt). The water cluster size distribution is slightly altered, such that pockets of <200 molecules are strongly favoured while the continuous network lies closely to the percolation threshold, forming fewer larger clusters. Despite the formation of discrete water pockets, the water–water coordination is mostly preserved with addition of guaiacol (Fig. S4 and Table S2†). The lysinate network is also slightly affected, leading to a preference for large but still finite aggregates.

Correlation functions in the [Ch][Lys]–water–guaiacol system show that hydrogen bonding with the guaiacol phenol group is the dominant solvent–solute interaction, and that interactions with its methoxy oxygen are negligible. This is in accordance with previous results for pyrrolidinium acetate and propylammonium nitrate ILs.[10]

Fig. 7A atom–atom correlation functions show that the guaiacol phenol forms shorter H-bonds with all three acceptor sites of the lysinate anion (1.0–2.2 Å) than it does with either water or the cation hydroxyl group (1.5–2.5 Å). Coordination numbers (Fig. 7B) show that H-bonding to the oxygens of water (0.20 ± 0.44) and carboxylate groups (0.21 ± 0.48) are most significant, but that bonding to ε-amino nitrogen is not negligible at 0.10 ± 0.30. This suggests that hydrogen bonding of guaiacol to both the carboxylate and ε-amine of lysinate facilitates its dissolution.

Fig. 7C and D shows the hydrogen bond-angle distributions and spatial distributions of multiple hydrogen bonding sites around the phenol group. Carboxylate oxygens (represented by the yellow lobe) lie exclusively in near-linear orientation next to the phenol hydrogen. This is also reflected in their H-bond-angle distributions around guaiacol (Fig. 7C), which are generally broader than for [Ch][Lys]–H_2O. Anion amino nitrogens (green and blue lobes) lie at slightly bent average positions, but the H-bonds from phenol to ε-amino (150–175°) are more linear, whereas those to the α-amino are mostly bent (140–160°) or very distorted (80–130°). H-Bonds between the phenol and water have a broad angular distribution. This is because water oxygens occupy multiple sites, including near-linear positions, bent positions, but are also seen next to the aromatic ring. Unlike choline phenylalaninate,[25] there is no evidence for cation–pi interactions between choline and guaiacol affecting solubility or local structure (see Fig. S3†). Both the bond angle distribution and the geometric arrangement of functional groups show a diverse range of hydrogen bonds around the guaiacol, which is different from the previously observed linear and directional interactions between guaiacol and simpler protic, alkylammonium ILs.[10] In the [Ch][Lys]–water mixture, there are more H-bonding capable species to interact with the guaiacol phenol group, yet these groups experience less competition geometrically.

In the simulation box (Fig. 4A), individual guaiacol molecules can be seen predominantly in contact with IL charged

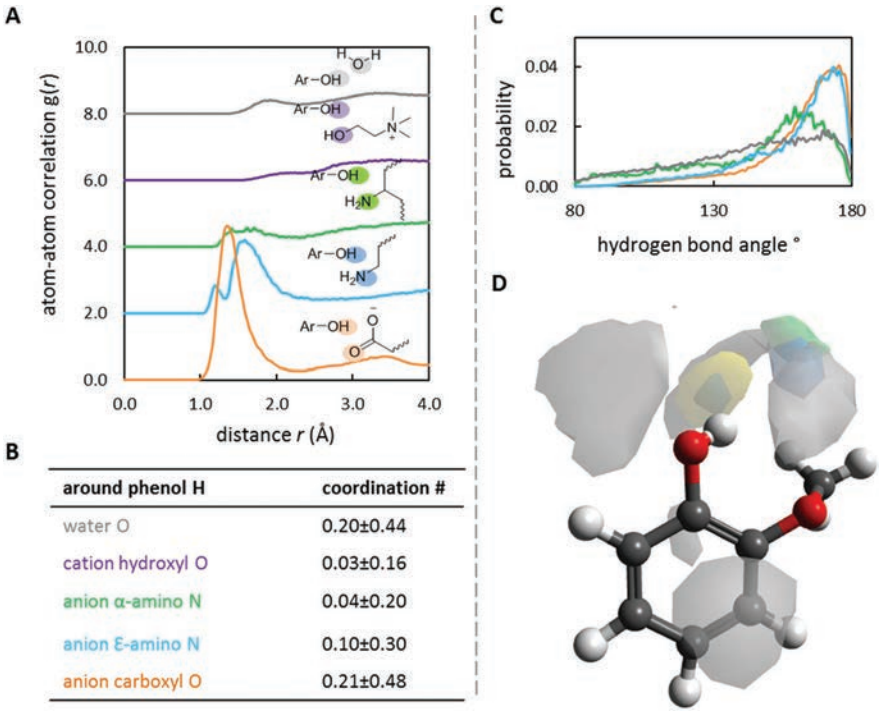

B

around phenol H	coordination #
water O	0.20±0.44
cation hydroxyl O	0.03±0.16
anion α-amino N	0.04±0.20
anion Ɛ-amino N	0.10±0.30
anion carboxyl O	0.21±0.48

Fig. 7 Key interactions around the phenol group in the [Ch][Lys]–water–guaiacol system. A. Atom–atom correlation functions, *g*(*r*). Three categories shown include water–guaiacol, cation–guaiacol and anion–guaiacol interactions. B. Coordination numbers at around phenol hydrogen, defined within 0–2.8 Å. C. Hydrogen bond angle distribution. D. 3D geometric plots show 20% probability surfaces. Plots and structural labels are colour matched.

(red) and uncharged groups (grey), but also with water (blue). This is consistent with the phenol H-bonding motifs identified above, and with some association of the aromatic ring at the interface between polar and non-polar domains formed within the IL. This is highly reminiscent of the preferred solubilisation site of aromatic solutes in the palisade layer of aqueous surfactant micelles.[35]

H-Bonding from the phenyl moiety in guaiacol to both the carboxyl and ε-amino lysinate acceptor sites significantly disrupts the ability of the anion to form its cyclic conformer (Fig. 3). While this has only a small effect on either the electrostatic or H-bond clusters in the [Ch][Lys]–water polar domains, or the existence of amphiphilic nanostructure (Fig. 4B), it reduces the methylenes' capacity to form a continuous non-polar network (Fig. 4B). In the presence of guaiacol, lysinate instead forms a broad distribution of large but finite aggregates with non-polar "cores" within a polar continuum. This strengthens the analogy with micelles, and underscores the significance of a flexible, heterogeneous, amphiphilic nanostructure in IL systems for solubilisation of organic solutes.[20]

Conclusions

Choline-based ILs and their aqueous solutions are economically viable and environmentally friendly solvents with promise in multiple applications, such as the conversion of lignocellulosic biomass into biofuels and bioproducts. The ability of some of these ILs to efficiently solubilize and fractionate lignin during pretreatment is advantageous in the production of high yields of fermentable sugars in a biorefinery. The cation–anion electrostatic correlation distance is much larger in choline lysinate than conventional protic or imidazolium ILs due to steric hindrance around the quaternary nitrogen, which also does not itself participate in H-bonding. The predominant interaction at short distances is instead between the choline hydroxyl group and the lysinate carboxylate. Decoupling H-bonding capacity from one charged site leads to those H-bonds that do form generally being short and linear,[24] also unlike conventional protic ILs.[36]

Surprisingly the lysinate sidechain allows [Ch][Lys] to adopt an amphiphilic nanostructure comprised of interpenetrating, bicontinuous domains of segregated charged and uncharged, non-polar moieties familiar in many ILs, but here the H-bonding network forms only finite clusters. Electrostatics primarily drives solvophobic self-assembly of non-polar groups into domains, which is assisted by the cyclisation of the lysinate. Addition of water (up to 26.5% w/w) does not significantly change the arrangement of cations and anions. Water forms a distribution of its own finite domains, which is contiguous with and forms H-bonds to the anion and to choline hydroxyl groups. This enables the IL H-bonds to rearrange into a continuous network without changing either the electrostatic or non-polar domain structures significantly. The structural

similarities between pure [Ch][Lys] and its water mixture explain its tolerance to added water without loss of functionality for various applications such as delignification, pre-treatment of coal, and the extraction of carbohydrate and lipids.[7,37]

A model aromatic solute such as guaiacol is readily accommodated into the solvent without disrupting the polar network structure. Compared to previously studied alkylammonium and pyrrolidinium ILs, choline lysinate has four distinct hydrogen bonding sites (hydroxyl, amino (×2), and carboxylate) through which to interact with phenolic compounds. In [Ch][Lys], the solvent–solute interactions experience less geometric competition at short distances. Not only do water molecules go next to H-bonding sites of guaiacol, they also distribute near the aromatic ring, facilitating its solubilisation. These features of [Ch][Lys] together with its amphiphilic nanostructure are important for aromatic dissolution and biomass processing.

Beyond liquid nanostructure and hydrogen bonding capacity, water mixtures of amino-acid based ILs are cheaper to use in industrial settings such as biorefineries as compared to anhydrous ILs, are potentially easier to recycle and less viscous, all of which have been key challenges for using ionic liquids at the industrial scale.[38] The presence of water also facilitates the measurement of pH, activity and conductivity. These physicochemical properties of ILs and their aqueous solutions are all important factors to consider for applications in biocatalysis, catalysis, cytoxicity and electrochemistry.[39]

Conflicts of interest

There are no conflicts to declare.

Acknowledgements

This work was supported by a Discovery Grant from the Australian Research Council. HJJ Acknowledges receipt of a Henry Bertie and Florence Mabel Gritton postgraduate scholarship, and SM an RTP scholarship from the Australian government. HJJ and SM acknowledge scholarships from the Australian Institute of Nuclear Science and Engineering. The neutron diffraction was performed at ISIS Neutron and Muon Source (RAL, UK), SANDALS beamline. BAS acknowledges support from the Joint BioEnergy Institute that is funded by the US Department of Energy, Office of Science, and Office of Biological and Environmental Research, through Contract DE-AC02-05CH11231 between Lawrence Berkeley National Laboratory and the US Department of Energy.

References

1 E. C. Achinivu, R. M. Howard, G. Q. Li, H. Gracz and W. A. Henderson, Lignin extraction from biomass with protic ionic liquids, *Green Chem.*, 2014, **16**(3), 1114–1119.
2 A. Brandt, J. Grasvik, J. P. Hallett and T. Welton, Deconstruction of lignocellulosic biomass with ionic liquids, *Green Chem.*, 2013, **15**(3), 550–583.
3 Q.-P. Liu, X.-D. Hou, N. Li and M.-H. Zong, Ionic liquids from renewable biomaterials: synthesis, characterization and application in the pretreatment of biomass, *Green Chem.*, 2012, **14**(2), 304–307.
4 H. Ren, M.-H. Zong, H. Wu and N. Li, Efficient Pretreatment of Wheat Straw Using Novel Renewable Cholinium Ionic Liquids To Improve Enzymatic Saccharification, *Ind. Eng. Chem. Res.*, 2016, **55**(6), 1788–1795.
5 X.-D. Hou, T. J. Smith, N. Li and M.-H. Zong, Novel renewable ionic liquids as highly effective solvents for pretreatment of rice straw biomass by selective removal of lignin, *Biotechnol. Bioeng.*, 2012, **109**(10), 2484–2493.
6 N. Sun, R. Parthasarathi, A. M. Socha, J. Shi, S. Zhang, V. Stavila, K. L. Sale, B. A. Simmons and S. Singh, Understanding pretreatment efficacy of four cholinium and imidazolium ionic liquids by chemistry and computation, *Green Chem.*, 2014, **16**(5), 2546–2557.
7 X.-D. Hou, N. Li and M.-H. Zong, Facile and Simple Pretreatment of Sugar Cane Bagasse without Size Reduction Using Renewable Ionic Liquids–Water Mixtures, *ACS Sustainable Chem. Eng.*, 2013, **1**(5), 519–526.
8 C. F. Carrozza, G. Papa, A. Citterio, R. Sebastiano, B. A. Simmons and S. Singh, One-pot bio-derived ionic liquid conversion followed by hydrogenolysis reaction for biomass valorization: A promising approach affecting the morphology and quality of lignin of switchgrass and poplar, *Bioresour. Technol.*, 2019, **294**, 122214.
9 H. J. Jiang, S. Imberti, R. Atkin and G. G. Warr, Dichotomous Well-defined Nanostructure with Weakly Arranged Ion Packing Explains the Solvency of Pyrrolidinium Acetate, *J. Phys. Chem. B*, 2017, **121**(27), 6610–6617.
10 H. J. Jiang, S. Imberti, B. A. Simmons, R. Atkin and G. G. Warr, Structural Design of Ionic Liquids for Optimizing Aromatic Dissolution, *ChemSusChem*, 2019, **12**(1), 270–274.
11 A. K. Soper, W. S. Howells and A. C. Hannon, *ATLAS: analysis of time-of-flight diffraction data from liquid and amorphous samples*, Rutherford Appleton Laboratory, Didcot, 1989.
12 A. K. Soper, W. S. Howells and A. C. Hannon, *ATLAS: analysis of time-of-flight diffraction data from liquid and amorphous samples*, Rutherford Appleton Laboratory, Didcot, 1989.
13 A. K. Soper, Empirical potential Monte Carlo simulation of fluid structure, *Chem. Phys.*, 1996, **202**, 295.
14 T. Youngs, https://www.projectaten.com/dlputils.
15 R. Hayes, S. Imberti, G. G. Warr and R. Atkin, Amphiphilicity determines nanostructure in protic ionic liquids, *Phys. Chem. Chem. Phys.*, 2011, **13**(8), 3237–3247.
16 R. Hayes, G. G. Warr and R. Atkin, Structure and Nanostructure in Ionic Liquids, *Chem. Rev.*, 2015, **115**(13), 6357–6426.

17 H. K. Kashyap, J. J. Hettige, H. V. R. Annapureddy and C. J. Margulis, SAXS anti-peaks reveal the length-scales of dual positive-negative and polar-apolar ordering in room-temperature ionic liquids, *Chem. Commun.*, 2012, **48**(42), 5103–5105.
18 A. Triolo, O. Russina, H. J. Bleif and E. DiCola, Nanoscale Segregation in Room Temperature Ionic Liquids, *J. Phys. Chem. B*, 2007, **111**(18), 4641–4644.
19 J. N. A. Canongia Lopes and A. A. H. Pádua, Nanostructural Organization in Ionic Liquids, *J. Phys. Chem. B*, 2006, **110**(7), 3330–3335.
20 S. Miao, R. Atkin and G. G. Warr, Amphiphilic nanostructure in choline carboxylate and amino acid ionic liquids and solutions, *Phys. Chem. Chem. Phys.*, 2020, **22**(6), 3490–3498.
21 M. Campetella, S. De Santis, R. Caminiti, P. Ballirano, C. Sadun, L. Tanzi and L. Gontrani, Is a medium-range order pre-peak possible for ionic liquids without an aliphatic chain?, *RSC Adv.*, 2015, **5**(63), 50938–50941.
22 M. Campetella, D. C. Martino, E. Scarpellini and L. Gontrani, Low-Q peak in X-ray patterns of choline-phenylalanine and -homophenylalanine: A combined effect of chain and stacking, *Chem. Phys. Lett.*, 2016, **660**, 99–101.
23 M. Campetella, E. Bodo, M. Montagna, S. De Santis and L. Gontrani, Theoretical study of ionic liquids based on the cholinium cation. Ab initiosimulations of their condensed phases, *J. Chem. Phys.*, 2016, **144**(10), 104504–104508.
24 M. Campetella, A. Le Donne, M. Daniele, L. Gontrani, S. Lupi, E. Bodo and F. Leonelli, Hydrogen Bonding Features in Cholinium-Based Protic Ionic Liquids from Molecular Dynamics Simulations, *J. Phys. Chem. B*, 2018, **122**(9), 2635–2645.
25 S. Miao, J. Wood, H. J. Jiang, S. Imberti, R. Atkin and G. Warr, Unusual origin of choline phenylalaninate ionic liquid nanostructure, *J. Mol. Liq.*, 2020, **319**, 114327.
26 R. Hayes, S. Imberti, G. G. Warr and R. Atkin, Effect of Cation Alkyl Chain Length and Anion Type on Protic Ionic Liquid Nanostructure, *J. Phys. Chem. C*, 2014, **118**, 13998–13998.
27 A. Henao, G. N. Ruiz, N. Steinke, S. Cerveny, R. Macovez, E. Guardia, S. Busch, S. E. McLain, C. D. Lorenz and L. C. Pardo, On the microscopic origin of the cryoprotective effect in lysine solutions, *Phys. Chem. Chem. Phys.*, 2020, **22**(13), 6919–6927.
28 R. Hayes, S. Imberti, G. G. Warr and R. Atkin, Pronounced sponge-like nanostructure in propylammonium nitrate, *Phys. Chem. Chem. Phys.*, 2011, **13**(30), 13544–13551.
29 N. Jan, Large lattice random site percolation, *Physica A*, 1999, **266**(1–4), 72–75.
30 R. Hayes, S. Imberti, G. G. Warr and R. Atkin, How Water Dissolves in Protic Ionic Liquids, *Angew. Chem., Int. Ed.*, 2012, **51**(30), 7468–7471.
31 A. K. Soper, The radial distribution functions of water and ice from 220 to 673 K and at pressures up to 400 MPa, *Chem. Phys.*, 2000, **258**(2–3), 121–137.
32 P. Varanasi, P. Singh, M. Auer, P. D. Adams, B. A. Simmons and S. Singh, Survey of renewable chemicals produced from lignocellulosic biomass during ionic liquid pretreatment, *Biotechnol. Biofuels*, 2013, **6**, 14.
33 Z. Sun, B. Fridrich, A. de Santi, S. Elangovan and K. Barta, Bright Side of Lignin Depolymerization: Toward New Platform Chemicals, *Chem. Rev.*, 2018, **118**(2), 614–678.
34 X. D. Hou, T. J. Smith, N. Li and M. H. Zong, Novel renewable ionic liquids as highly effective solvents for pretreatment of rice straw biomass by selective removal of lignin, *Biotechnol. Bioeng.*, 2012, **109**(10), 2484–2493.
35 M. Almgren, F. Grieser and J. K. Thomas, Dynamic and Static Aspects of Solubilization of Neutral Arenes in Ionic Micellar Solutions, *J. Am. Chem. Soc.*, 1979, **101**, 279–291.
36 R. Hayes, S. Imberti, G. G. Warr and R. Atkin, The Nature of Hydrogen Bonding in Protic Ionic Liquids, *Angew. Chem., Int. Ed.*, 2013, **52**(17), 4623–4627.
37 T. Q. To, K. Procter, B. A. Simmons, S. Subashchandrabose and R. Atkin, Low cost ionic liquid-water mixtures for effective extraction of carbohydrate and lipid from algae, *Faraday Discuss.*, 2018, **206**, 93–112.
38 S. H. Mood, A. H. Golfeshan, M. Tabatabaei, G. S. Jouzani, G. H. Najafi, M. Gholami and M. Ardjmand, Lignocellulosic biomass to bioethanol, a comprehensive review with a focus on pretreatment, *Renewable Sustainable Energy Rev.*, 2013, **27**, 77–93.
39 T. L. Greaves and C. J. Drummond, Protic Ionic Liquids: Evolving Structure-Property Relationships and Expanding Applications, *Chem. Rev.*, 2015, **115**(20), 11379–11448.

